OBSERVATION OF AN ISOKINETIC TEMPERATURE AND COMPENSATION EFFECT FOR HIGH TEMPERATURE CRUDE OIL FOULING

C. A. Bennett[1], **R. S. Kistler**[2], **K. Nangia**[3], **W. Al-Ghawas**[4], **N. Al-Hajji**[5], and **A. Al-Jemaz**[6]

[1] Heat Transfer Research, Inc., College Station, Texas, USA, CAB@HTRI.net
[2] Heat Transfer Research, Inc., College Station, Texas, USA, RSK@HTRI.net
[3] Fluor Corporation, Aliso Viejo, California, USA, Krish.Nangia@Fluor.com
[4] KNPC, Kuwait, W.Ghawas@KNPC.com
[5] KNPC, Kuwait, N.Yousef@KNPC.com
[6] KNPC, Kuwait, A.Jemaz@KNPC.com

ABSTRACT

The initial fouling rates of four crude oils were determined at a nominal bulk temperature of 315 °C, an initial heated wall shear stress of 13 Pa, and initial surface temperatures between 375 and 445 °C. These initial fouling rates ranged from $1.3(10^{-6})$ to $7.8(10^{-5})$ m^2 K/kJ. Corresponding Arrhenius plots were linear with the initial fouling rates passing through an isokinetic temperature of 407.5 °C. A plot of the natural logarithm of the pre-exponential factors $(7.6(10^4) - 5.2(10^{15}))$ m^2 K/kJ versus the apparent activation energies (128 – 269 kJ/mol) was also linear, confirming the validity of the isokinetic temperature and the presence of the compensation effect. Below the isokinetic temperature, the relative fouling rates were Crude Oil C > Crude Oil A > Crude Oil D > Crude Oil B; above the isokinetic temperature, the relative fouling rates were reversed (Crude Oil B > Crude Oil D > Crude Oil A > Crude Oil C). Chemical characterization of a fouling deposit suggested that the dominant fouling mechanism at these conditions was coking with significant contributions from sedimentation (iron sulfide) and corrosion (~340 µm/yr) of the 304 stainless steel test material.

INTRODUCTION

Yeap et al. (2004) provide an excellent description of crude oil preheat, distillation, and fouling:

- Crude oil distillation is a significant consumer of energy, requiring roughly 4% of the total equivalent energy of the crude oil.
- Energy is recovered with the preheat train, but at best the process is only 60 – 70% efficient.
- Fouling of the crude oil preheat train heat exchangers results in further diminished heat transfer efficiency.

Yeap et al. (2004) also cite the earlier estimate of Panchal (1995) that, in the U.S. alone, fouling in crude oil distillation units costs about $1.3 billion per year. It should be noted that fouling concomitantly increases greenhouse gas emissions. Considering the above, it is clearly imperative for industry to understand and mitigate this challenging problem.

The dominant fouling mechanism varies with location along the crude oil preheat train. Prior to the desalter, fouling occurs predominantly via salt crystallization and sedimentation. At the end of the preheat train, fouling is primarily due to asphaltene adhesion to the heat transfer surface. In the fired heater, coking is the prevailing fouling mechanism. Corrosion—being a function of crude oil chemistry, temperature, and metallurgy—can happen throughout the preheat train.

Owing to the multiple mechanisms involved, crude oil fouling is very complex. Further complicating matters is the fact that for several mechanisms (asphaltene adhesion, coking, and corrosion), the fouling behavior varies significantly with crude oil composition. A means of simplifying the analysis, such as finding common factors, would be beneficial.

Although neither well understood nor universally accepted, the isokinetic phenomenon is nevertheless well documented (Yelon et al., 2006; Linert et al., 1983; Schneider and Mayr, 1986; Somorjai, 1994). The isokinetic phenomenon has perhaps been most aptly described by Yelon et al. (2006) as "the frequent observation that the amplitude of the prefactor to the exponential term in the Arrhenius equation increases exponentially as the activation energy increases." As a result, there is a mathematical relationship between the pre-exponential factor and the apparent activation energy (Somorjai, 1994):

$$\ln A = \alpha + \frac{E}{RT_{iso}} \qquad (1)$$

A plot of ln A versus E will subsequently be called a compensation effect plot. T_{iso}, the isokinetic temperature, is the temperature at which the chemical reaction (i.e., fouling) rates are all equal, and on an Arrhenius plot is the temperature at which the rates are within experimental error.

Industry-recommended procedures for crude oil preheat fouling research (Bennett et al., 2006) were followed in all aspects of this work.

Table 1. Crude Oil (A – E) Assays

Property, Analysis Method, Units	A	B	C	D	E
Kinematic viscosity (37.8 °C), D-445, mm^2/s	154.4	33.0	286.1	11.77	24.52
Kinematic viscosity (40.0 °C), D-445, mm^2/s	137.4	30.2	246.9	11.06	—
Kinematic viscosity (50.0 °C), D-445, mm^2/s	84.2	20.9	134.4	8.51	17.04
Specific gravity (15.6/15.6 °C), D-5002, —	0.9469	0.9092	0.9731	0.8784	0.9101
Characterization factor, UOP-375, —	11.5	11.7	—	11.6	11.7
Total acidity, D-664, mg KOH/g crude oil	0.37	0.07	0.92	0.06	0.56
Salt content, D-3230, lb/1000 bbl	9.4	17.1	50.5	4.1	—
Carbon residue, D-4530, % mass	10.86	9.55	(D-189) 10.90	6.35	(D-189) 7.31
Sulfur, D-2622, % mass	4.7	3.8	(IP-336) 5.33	2.75	(D-4294) 1.81
Mercaptan sulfur, UOP-163, mg/kg	70	147	381	120	—
H$_2$S, UOP-163, mg/kg	66	110	—	< 3	—
Basic nitrogen, UOP 269, mg/kg	470	480	(CBA-73) 570	370	553
Nickel, E DIN 51790-7, mg/kg	21	22	(CBA-21) 24.8	11	(D-5708) 38
Vanadium, E DIN 51790-7, mg/kg	59	49	(CBA-21) 89.3	35	(D-5708) 104
Iron, —, mg/kg	—	—	(CBA-21) 17	—	(D-5708) 10
Saturates, —, % mass	24.87	26.61	18.40	33.82	35.29
Aromatics, —, % mass	55.07	51.10	56.75	49.10	46.58
Resins, —, % mass	12.24	13.88	15.11	13.09	10.08
Asphaltenes, —, % mass	7.82	8.40	9.74	3.99	8.05
Colloidal instability index (*CII*)	0.486	0.539	0.392	0.608	0.765

Fig. 1 HTFU

METHODS AND MATERIALS

Crude Oils

Five crude oils were studied in this work: Crude Oils A – D were investigated under contract for Fluor and KNPC, and Crude Oil E was donated by the HTRI Crude Oil Fouling Task Force (COFTF). Nitrogen was bubbled through the crude oils for four hours upon receipt and 30 minutes after each sample was taken to remove dissolved

Table 2. Operational Maxima of the HTFU

Bulk temperature	315 °C
Initial surface temperature	450 °C
Pressure	6.9 MPa
Charge	25 L
Pump flow rate	3.4 m^3/hr
Test section velocity	4 m/s

oxygen. The assays of these nitrogen-saturated crude oils are provided in Table 1. Crude Oils A – D were characterized by PetroTech Intel, whereas Crude Oil E was characterized by Core Laboratories. Colloidal instability index (*CII*) was calculated using Equation (2) (Por, 1992).

$$CII = \frac{saturates + asphaltenes}{resins + aromatics} \tag{2}$$

High Temperature Fouling Unit (HTFU)

The fouling experiments were performed with the HTRI HTFU (Fig. 1). Operational limits of the HTFU are provided in Table 2. Note from Fig. 1 that the pump discharge manifold has three hydraulically equivalent outlets to ensure even distribution of particulate matter. Furthermore, calculations based upon the properties of an average   crude
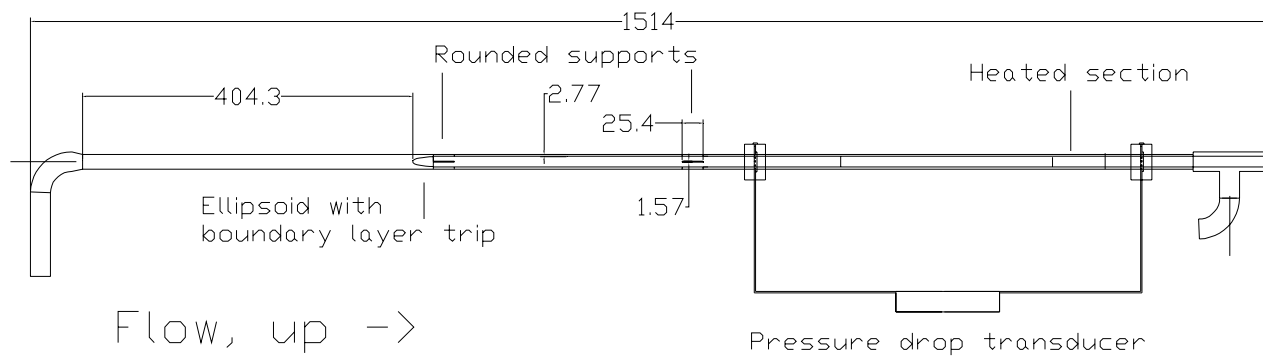
Fig. 2 Test section schematic. Dimensions are given in mm

Fig. 3 Photograph of uninsulated HTFU test sections without pressure drop transducers implemented

oil reveal that the Reynolds number in the common piping is on the order of 100 000 at experimental conditions, which is sufficiently turbulent to keep typical particulate matter suspended. The HTFU has two identical test sections and a bypass. The test sections are illustrated schematically in Fig. 2 and photographically in Fig. 3. Starting at the inlet on the left of Fig. 2, flow enters the test section and proceeds through 22.2 hydraulic diameters of vertically oriented open pipe. Even distribution of particulate matter is ensured by means of turbulent mixing, which was confirmed with computational fluid dynamics (CFD) (Fig. 4). Next, an ellipsoid provides an even transition from tubular to annular flow. The annular gap is 2.77 mm. Then the flow passes into the annular extension, which is supported by a total of eight rounded supports that are 25.4 mm long by 1.57 mm wide. The remainder of the annulus is formed by the HTRI fouling probe itself, described below. CFD, performed under isothermal conditions, confirmed that the 132 hydraulic diameters of flow development length yield fully developed flow and less than 5% variation in shear stress over the heated section in the range 42 < Re < 42 000 (Fig. 5).

The HTRI fouling probe is shown photographically in Fig. 6 and schematically in Fig. 7. The heart of the probe is a Watlow FIREROD® heater cartridge. This heater cartridge is encased in a copper tube for even heat distribution. Four K-type thermocouples are placed at 90° intervals around the outer circumference of the copper tube. Mica fills the rod outside the heated region. Finally, the assembly is swaged into a sheath; we used 304 stainless steel for this study. CFD has shown that the axial heat losses from the 101.6 mm long heated section are less than 5% of the duty. Thermal resistances between the embedded thermocouples and the outer surface of the sheath were calibrated using a modification of the Wilson (1915) technique. These calibrated resistances were subsequently used to calculate the temperatures of the sheath surface with Equation (3).

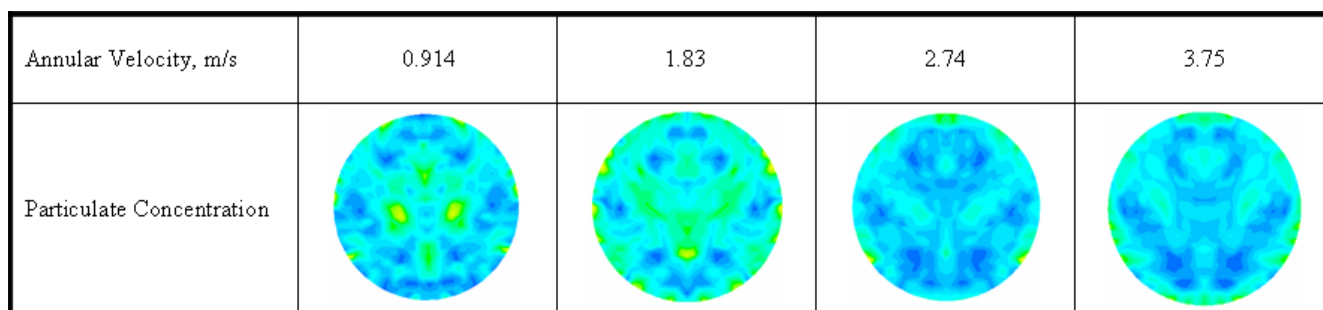| Annular Velocity, m/s	0.914	1.83	2.74	3.75
Particulate Concentration				

Fig. 4 Particulate matter distribution just before entering the annulus as a function of velocity from CFD
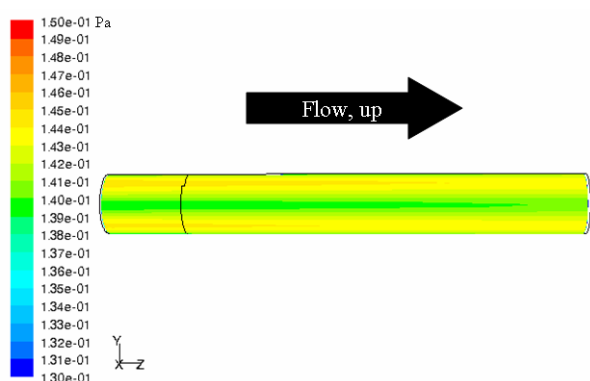

Fig. 5 Shear stress at the fouling probe heated section wall from CFD
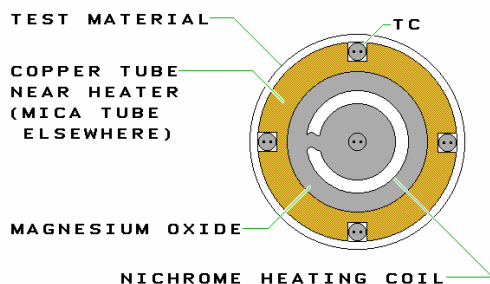

Fig. 6 HTRI fouling probe

Fig. 7 Schematic of HTRI fouling probe

$$T_s = T_{imb} - qR_s \qquad (3)$$

Fouling resistance was then computed with Equation (4).

$$R_f = \left(\frac{T_s - T_b}{q} \right)_t - \left(\frac{T_s - T_b}{q} \right)_{t=0} \qquad (4)$$

Experimental Design

The primary objective of this work was to emulate, within the operational limits of the HTFU, fouling in the atmospheric distillation column fired heater. Of secondary interest was fouling at the end of the crude oil preheat train. The four crude oils investigated in this part of the study were

1. Crude Oil A
2. Crude Oil B
3. Crude Oil C
4. Crude Oil D

Crude Oil A was given the highest priority because, based on limited operational experience, it was known to foul heavily at the end of the crude oil preheat train. The fouling propensities of Crude Oils B and C were not known. Because the operator (KNPC) had extensive experience processing Crude Oil D, it had the lowest priority and served as the baseline.

The experimental design is provided in Table 3. Experiments were designed to yield 13 Pa of shear stress at the heated surface (Fig. 8), calculated using the method compiled by Bhatti and Shah (1987), at a nominal bulk temperature of 315 °C. This wall shear stress corresponds to Crude Oil A flowing at an average velocity of 2.74 m/s at a bulk temperature of 315 °C in an N6 S40 pipe with a surface roughness of 20 μm.

Experimental Operation

The HTFU was cleaned carefully between experiments. Fouling deposits were removed from the surface of the rod with an aluminum tool and the sheath was polished with an alumina-impregnated nylon pad (280 grit). P-xylene was

Table 3. Experimental Design

			Test Section 1			Test Section 2		
Run	Crude Oil	T_b, °C	Metal[a]	$T_{s,ini}$, °C	V[b], m/s	Metal[a]	$T_{s,ini}$, °C	V[b], m/s
1	A	315	304SS	377	1.65	304SS	399	1.65
2	B	315	304SS	377	1.84	304SS	399	1.84
3	C	315	304SS	377	2.16	304SS	399	2.16
4	D	315	304SS	377	2.13	304SS	443	2.13
5	D	315	304SS	421	2.13	304SS	399	2.13
6	A	315	304SS	421	1.65	304SS	443	1.65
7	C	315	304SS	421	1.84	304SS	443	1.84
8	B	315	304SS	421	2.16	304SS	443	2.16

[a] 304 stainless steel was the most germane metal available in the time frame allotted; future work on crude oil fouling at atmospheric distillation column fired heater conditions should consider employing 347 stainless steel

[b] These velocities yield a shear stress of 13 Pa on the inner surface of the annulus
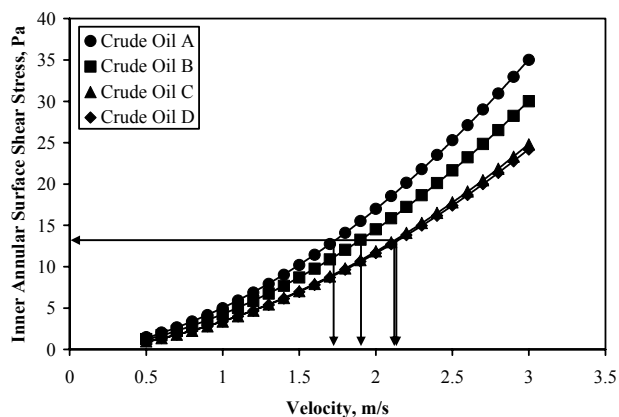

Fig. 8 Shear stress on the heated surface of the annulus for the four crude oils tested at a bulk temperature of 315 °C

circulated through the unit, with the valves being cycled, for at least an hour. Then the p-xylene was purged and a charge of the crude oil to be studied was circulated through the unit, again cycling the valves, for at least an hour to remove the p-xylene. The wash crude oil was then purged from the HTFU. Finally, the HTFU was charged with the crude oil to be studied.

The electric heat trace for bulk temperature control was set to 315 °C, but power was added to the rods at a bulk temperature of 305 °C so that the power input from the rods would quickly bring the bulk temperature to 315 °C without significantly overshooting the bulk temperature set-point. Power was added to the rods until the desired surface temperature (calculated in real time by LabVIEW®) was reached, which was taken as time zero for Equation (4). Experiments were terminated when either the rod core temperature reached 925 °C or eight hours had elapsed, whichever came first.

Fouling Deposit Characterization

Fouling deposits produced from the runs shown in Table 3 were not characterized. Instead, a fouling deposit was produced by fouling Crude Oil E at a bulk temperature of 320 °C, an initial surface temperature of 370 °C, an initial heated surface shear stress of 13 Pa, and a static pressure of 5.8 MPa for 72 hours. The deposit was collected with an aluminum tool. The characterization was performed by Material Interface, Inc. Prior to characterization, the fouling deposit was washed three times with toluene, followed by three washings with n-heptane to remove the pervasive crude oil. The fouling deposit was then dried at 110 °C in flowing ultra-high-purity helium for 12 hours. Future work will utilize the Oil Compatibility Model (Wiehe and Kennedy, 2000a; Wiehe and Kennedy, 2000b) for selecting the solvents used to wash the fouling deposits in an endeavor to remove the crude oil without dissolving the adhered asphaltenes. We can only speculate that this fouling deposit is representative for these experimental conditions; future work will be more characterization intensive.

Scanning Electron Microscopy (SEM))/Energy Dispersive Spectroscopy (EDS). SEM/EDS was performed with a JEOL JSM 35C instrument equipped with a thin window, light element detector. The primary voltage used for the analysis was 25 kV. Traditional SEM images were obtained, with the major contrast mechanism being topographic in nature. The EDS detector used could not detect nitrogen. A particle size analysis was performed by suspending a sample in a volatile solvent, ultrasonically mixing it, and applying it to a copper substrate. Particle size counting was accomplished from a binary image. Because the SEM analysis revealed that the sample was heterogeneous, all subsequent characterizations were performed on a sample that was ground and well mixed.

Table 4. Experimental Results

Run	Crude Oil	Test Section 1						Test Section 2					
		T_b, °C	$T_{s,ini}$, °C	V, m/s	Re^a	Pr^a	$(dR_f/dt)_{ini}^b$, m^2 K/kJ	T_b, °C	$T_{s,ini}$, °C	V, m/s	Re^a	Pr^a	$(dR_f/dt)_{ini}^b$, m^2 K/kJ
1	A	316	375	1.65	$1.58(10^5)$	1.89	$3.9(10^{-6})$	316	409	1.65	$1.59(10^5)$	1.88	$4.6(10^{-6})^c$
2	B	316	377	1.83	$1.10(10^5)$	2.97	$1.3(10^{-6})$	317	398	1.83	$1.12(10^5)$	2.93	$6.4(10^{-6})$
3	C	315	378	2.16	$5.32(10^4)$	7.55	Negative	317	400	2.16	$5.44(10^4)$	7.41	$1.3(10^{-5})$
4	D	315	377	2.13	$6.85(10^4)$	5.38	$2.3(10^{-6})$	Rod failed before experiment began					
5	D	323	360	2.13	$7.22(10^4)$	5.17	$7.3(10^{-6})^c$	323	424	2.13	$7.25(10^4)$	5.15	$2.4(10^{-5})$
6	A	317	391	1.65	$1.60(10^5)$	1.87	$1.9(10^{-5})$	317	446	1.65	$1.60(10^5)$	1.87	$5.4(10^{-5})$
7	C	320	391	2.16	$5.68(10^4)$	7.14	$4.8(10^{-6})$	320	442	2.16	$5.68(10^4)$	7.14	$3.1(10^{-5})$
8	B	319	426	1.83	$1.14(10^5)$	2.88	$4.1(10^{-5})$	319	436	1.83	$1.14(10^5)$	2.88	$7.8(10^{-5})$

[a] Reynolds and Prandtl numbers based on fluid properties evaluated at the bulk temperature

[b] Initial fouling rates based on the maximum $\dfrac{dR_f}{dt}$ in regions of $\dfrac{d^2 R_f}{dt^2} = 0$
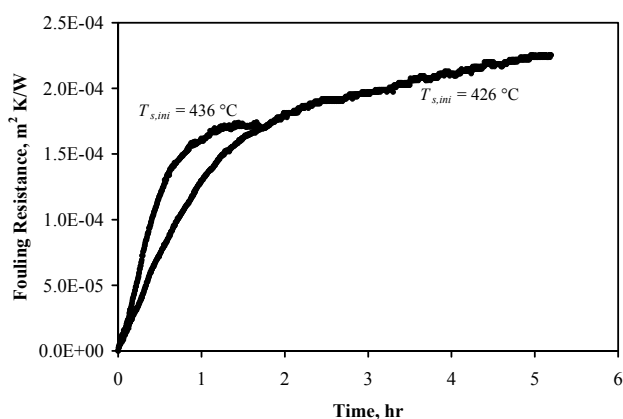
[c] Anomalous data point

Fig. 9 Fouling resistance versus time for run 8

Combustion Analysis. Carbon, hydrogen, and nitrogen were measured using an Exeter Analytical CE440 elemental analyzer in accord with ASTM D-5373. Sulfur was measured with a Leco SC-632 sulfur analyzer in accord with ASTM D-4239.

Thermal Gravimetric Analysis (TGA). TGA was performed with a TA Instruments AutoTGA 2950HR. The sample was suspended in flowing ultra-high-purity helium and heated from room temperature to 110 °C at 10 °C/min, held at 110 °C for one hour, then heated to 900 °C at 10 °C/min and held at 900 °C for 10 minutes, then the flowing gas was switched to air and the sample was held at 900 °C for one hour.

X-Ray Diffraction (XRD). XRD was performed with a Rigaku Ultima III instrument. The incident radiation was Cu Kα at 44 kV and 40 mA.

Fourier Transform Infrared Spectroscopy (FTIR). The FTIR was performed with a Nicolet Model 6700

system equipped with a Smart Orbit diamond substrate ATR accessory. The sample was placed directly upon the diamond holder. The spectrum represents the average of 32 individual scans possessing spectral resolution of 4 cm^{-1}.

RESULTS

Crude Oil Fouling

Fig. 9 is a typical plot of fouling resistance versus time. Initial fouling rates were calculated from data in regions of maximum slope with no curvature. It is significant that the rod with an initial surface temperature of 426 °C continued fouling after the rod with an initial surface temperature of 436 °C reached an asymptotic fouling resistance; this indicates that the asymptotic approach was not due to fouling precursor depletion. We speculate that the asymptotic approach was due to the increasing surface roughness yielding a critical shear stress above which the fouling abated.

The results of the crude oil fouling experiments are tabulated in Table 4. Comparison of Tables 3 and 4 reveals that the actual experiments conformed closely to the experimental designs. Reynolds numbers were calculated using the hydraulic diameter of the annulus. Initial fouling rates ranged from $1.3(10^{-6})$ to $7.8(10^{-5})$ m^2 K/kJ. The initial fouling rate for run 3, test section 1, was negative and is not suitable for further data regression.

Fig. 10, a plot of the initial fouling rates versus the initial surface temperatures, points out two questionable data points. The test section 1 rod failed during run 5, resulting in an anomalous initial fouling rate. The run 1 test section 2 fouling resistance versus time plot never reached a region of zero second derivative, resulting in an aberrantly low fouling rate. These two points are not suitable for further data regression. The remaining initial fouling rates of Fig. 10 clearly demonstrate an exponential temperature dependence, indicating a chemical reaction fouling
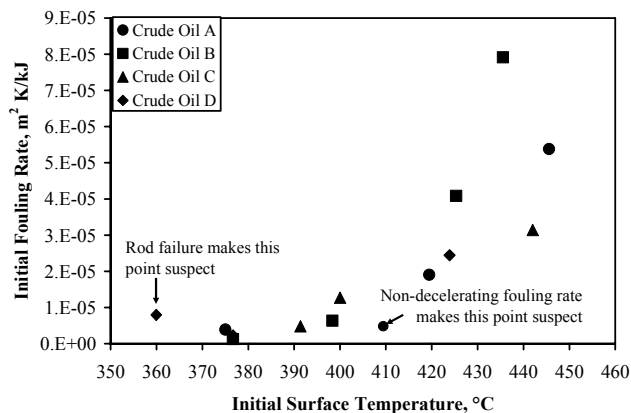
mechanism.

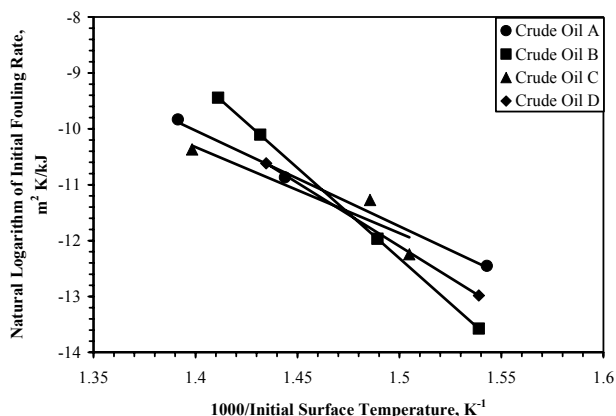Fig. 10 Initial fouling rates versus initial surface temperature

Fig. 11 Arrhenius plot

Table 5. Kinetic Parameters

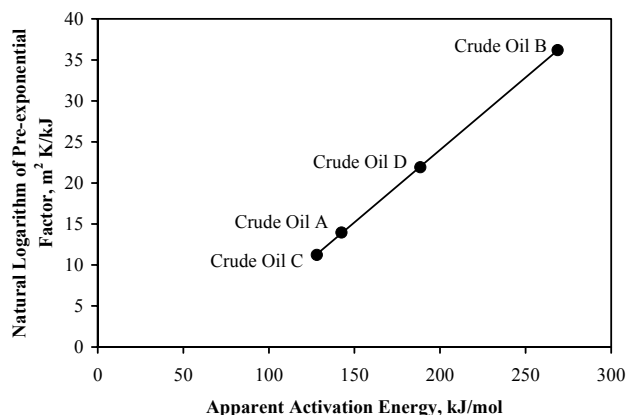| Crude Oil	E, kJ/mol	A, m^2 K/kJ
A	142	$1.15(10^6)$
B	269	$5.21(10^{15})$
C	128	$7.58(10^4)$
D	189	$3.31(10^9)$

Fig. 12 Compensation effect plot

Fig. 11 is an Arrhenius plot of the initial fouling rate versus the initial surface temperature. It should be noted that because the experiments were conducted under constant heat flux conditions, the temperature of the interface between the fouling deposit and the crude oil remained approximately constant at the initial surface temperature throughout the course of the experiment. Apparent activation energies and pre-exponential factors extracted from the Arrhenius plot are provided in Table 5. Recall that the experiments were designed to yield a constant initial shear stress at the heated surface of 13 Pa. We believe that operation at constant velocity or constant Reynolds number conditions, within the ranges presented in Table 4, would yield a very similar Arrhenius plot because the magnitudes of the apparent activation energies strongly suggest that these experiments were within the kinetically-controlled regime.

Fig. 12 is the compensation effect plot of Equation (1) using the data from Table 5. From Fig. 12, T_{iso} = 407.5 °C and α = -11.32.

Below the isokinetic temperature, the relative initial fouling rates were Crude Oil C > Crude Oil A > Crude Oil D > Crude Oil B; above the isokinetic temperature, the relative initial fouling rates were reversed (Crude Oil B > Crude Oil D > Crude Oil A > Crude Oil C).

Fouling Deposit Characterization

Scanning Electron Microscopy. The SEM revealed that the deposit had two general morphologies, a shiny black surface adjacent to the fouling rod sheath and a matte black surface at the interface with the crude oil. Fig. 13 is a micrograph of the dull matte surface and reveals that it was pocked with pores that were roughly 10 μm in diameter. Fig. 14 is a micrograph of the shiny black surface and demonstrates that it was also highly porous, but the pores were on the order of 1 μm in diameter. Given that the sheath surface temperature reached 600 °C by the end of the

experiment, sintering of the fouling deposit was not unexpected. Both the experimental conditions and the elemental analysis discussed below suggest that coking, and thus gas evolution, were expected (Savage et al., 1985). Boiling might also have occurred despite the high pressure. The particle size analysis revealed that all particles were between 0.5 and 10 μm in diameter, with 90% of them being less than 5 μm in diameter, and 56% of them between 1 and 5 μm in diameter (assuming spherical morphology).

Elemental Analysis. The results of the elemental analysis are provided in Table 6. Carbon, hydrogen, nitrogen, and sulfur were obtained by combustion, and the other elements were measured by EDS. Reported values are the average of three runs.

Table 6. Elemental Analysis of the Fouling Deposit Created from Crude Oil E[a, b]

C	51.17	Fe	21.4 (20.79[c])	Al	0.1	Co	0.1
H	1.48	Ni	3.8	Si	0.4	Zn	0.2
N	1.13	V	0.3	Ca	0.1	Mo	0.8
S	17.32 (18.58[c])	Cr	0.8	Mn	0.0	Total	99.1

[a] All quantities given in weight percent
[b] C, H, N, and S obtained from sample combustion, remainder from EDS, except where noted
[c] Value obtained from inductively coupled plasma – optical emission spectroscopy (ICP-OES)
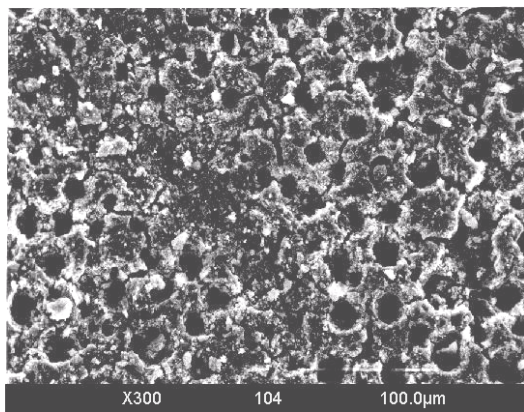

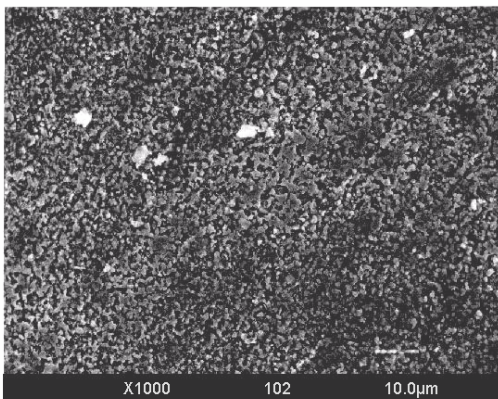Fig. 13 SEM micrograph of fouling deposit matte surface

Fig. 14 SEM micrograph of fouling deposit shiny surface

Inductively coupled plasma – optical emission spectroscopy (ICP-OES) was used to spot-check the iron and sulfur contents. The elemental analysis results were normalized to the sulfur content from combustion. The atomic hydrogen to carbon ratio of H/C = 0.345 is in the range reported for coke (Wiehe, 2001). Assuming the chromium originated with corrosion of the 304 stainless steel sheath, a corrosion rate of 340 μm/yr was estimated, which agreed reasonably well with the sulfur-corrected modified McConomy prediction (Kane, 2006) of 290 μm/yr. Based on the difference between 100% and the total from Table 6, the oxygen content of the sample was approximately 0.9%, demonstrating that the fouling deposit formed under these conditions was not a gum (Watkinson, 2007).

Thermal Gravimetric Analysis. The TGA results are provided in Fig. 15. The weight loss from room temperature through the hold at 110 °C was negligible, indicating that

the washed fouling deposit was completely dry. The fouling deposit began to lose mass at 190 °C and lost 2.28 wt% by the time the hold at 900 °C in ultra-high-purity helium finished. Upon switching the flowing gas to air, the sample rapidly combusted, leaving behind 32.8 wt% ash. This amount of ash was not unexpected given that Crude Oil E had 0.02 wt% sediment by extraction and was well mixed prior to charging the HTFU.
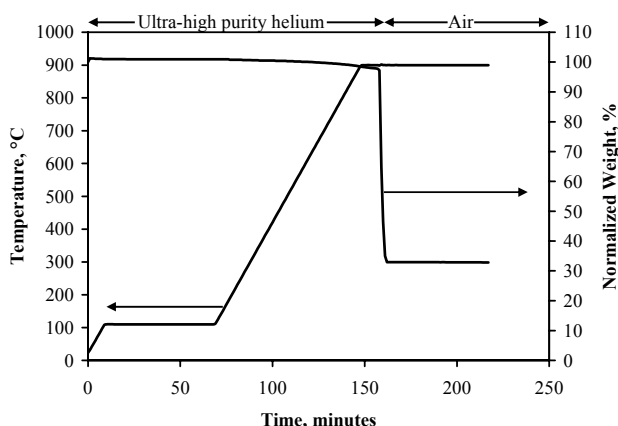

Fig. 15 Thermal gravimetric analysis of fouling deposit

X-Ray Diffraction. The XRD pattern of the fouling deposit is illustrated in Fig. 16. The primary phase was well matched by both FeS and $Fe_{1-x}S$. Based on the Fe-S phase diagram, $Fe_{1-x}S$ is likely the better match. The source of the $Fe_{1-x}S$ was probably the crude oil sediment; XRD will be performed on the sediment extracted from crude oils studied in the future. Pentlandite ($Fe_9Ni_9S_{16}$), also observed as a secondary crystalline phase, might have been a corrosion product.

Fourier Transform Infrared Spectroscopy. The FTIR spectrum collected from the fouling deposit is presented in
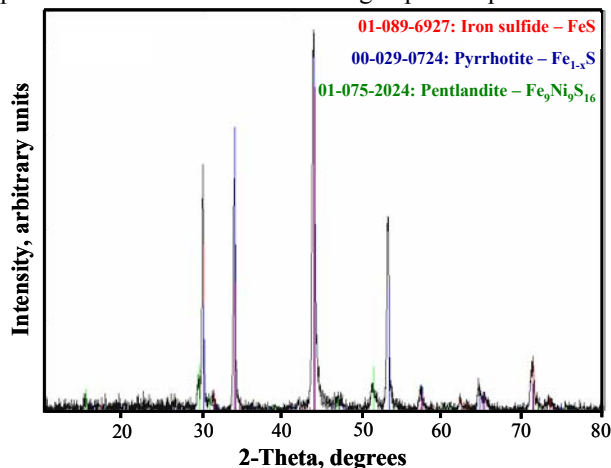

Fig. 16 X-ray diffraction pattern of fouling deposit showing the best powder diffraction file matches
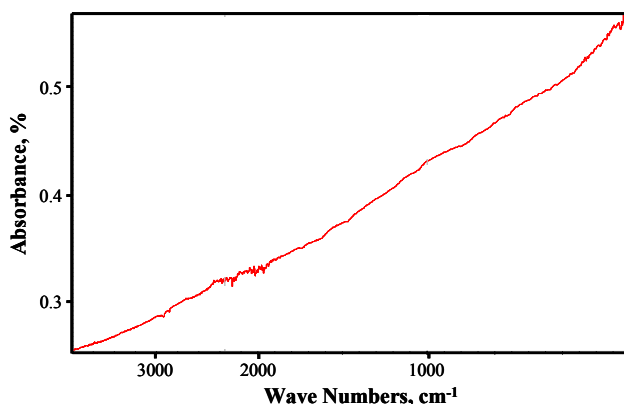

Fig. 17 Fouling deposit Fourier transform infrared spectrum

Fig. 17. There was no significant absorbance despite the 32 scans being run at maximum power. This result can be reconciled with the elemental analysis data by recognizing that the fouling deposit was graphitic in nature and had the nonmetals absorbed interstitially. Indeed, graphite is renowned for its hydrogen storage capacity (Park et al., 1998), and the graphitic nature of high temperature fouling deposits has been argued before (Fan and Watkinson, 2006). The absence of a graphite peak in the XRD pattern indicates that the sample was not true graphite.

DISCUSSION

The fouling deposit characterization suggests that three fouling mechanisms were active at these experimental conditions. The TGA and the elemental analysis suggest that coking was the dominant fouling mechanism. The TGA and the XRD suggest that sedimentation was also significant. Finally, the elemental analysis suggests that corrosion of the 304 stainless steel sheath occurred at an appreciable rate.

Because coking appeared to be the dominant fouling mechanism at these experimental conditions, the apparent activation energies reported in Table 5 should compare favorably with those in the literature, and indeed they do. Olmstead and Freund (1998) reported 217 kJ/mol for the coking of Arabian Heavy residuum. It should be noted that the large apparent activation energies reported in Table 5 strongly suggest that the fouling was kinetically limited, which was expected given the high Reynolds numbers employed in this work.

Perhaps the most striking result of this study is the observation that the initial fouling rates presented in the Arrhenius plot (Fig. 11) exhibit an isokinetic temperature; in other words, the initial fouling rates of the four crude oils are within experimental error (± 20%) at 407.5 °C. Although the isokinetic phenomenon has been observed for many chemical, biological, geological, and condensed matter systems (Yelon et al., 2006), this is, to the best of our

knowledge, the first time it has been reported for crude oil fouling.

An important feature of the isokinetic phenomenon is that it is general to entire classes of chemical reactions (Schneider and Mayr, 1986). This characteristic suggests that all crude oils might foul at roughly the same rate at 407.5 °C. If this assertion proves to be true, its applicability depends on the rate-limiting step. What then was the rate-limiting step for the fouling of this study—coking or asphaltene adhesion? Based on Wiehe (1992, 1993), we believe that the fouling likely progressed according to the following simplified sequence: maltene ↔ asphaltene ↔ asphaltene adhesion to the heat transfer surface → coking reactions. According to Watkinson (2007), the adhesion of the asphaltenes to the heat transfer surface could have been rate-limiting. As a result, the isokinetic phenomenon might apply to asphaltene adhesion fouling in addition to coking.

The compensation effect has modeling ramifications. At present, there are many fouling models in the open literature. Nearly all of these models lump the pre-exponential factor into a "constant." Table 5 clearly demonstrates that the pre-exponential factor varies dramatically with various crude oils. As a result, we suggest that models explicitly account for the pre-exponential factor. Moreover, once apparent activation energy is correlated, calculation of the pre-exponential factor will be possible with Equation (1) for relevant fouling mechanisms.

We knew at the outset of this work that Crude Oil A was a heavy fouler at the end of the preheat train. Projecting the initial fouling rates, using Fig. 11, to an initial surface temperature of 260 °C, we found that Crude Oil A fouls at roughly 1000% the rate of Crude Oil D. This finding parallels operational experience, thereby supporting our conjecture that the rate-limiting step was asphaltene adhesion. Similarly, Crude Oil C is expected to foul at roughly 1800% the rate of Crude Oil D at 260 °C, whereas Crude Oil B would foul roughly 95% slower.

The reversal of the relative initial fouling rates above and below the isokinetic temperature is noteworthy. It suggests that crude oils that foul most heavily in the preheat train could foul less severely than their peers in the atmospheric distillation column fired heater. Conversely, crude oils that foul less severely than their peers in the preheat train could be problematic in the fired heater. Additional research on the isokinetic phenomenon of crude oil fouling is needed.

CONCLUSIONS
1. An isokinetic temperature was observed at 407.5 °C.
2. The compensation effect permits calculation of the pre-exponential factor from the apparent activation energy.
3. Below the isokinetic temperature, the relative fouling rates were Crude Oil C > Crude Oil A > Crude Oil D > Crude Oil B; above the isokinetic temperature, the

relative fouling rates were reversed (Crude Oil B > Crude Oil D > Crude Oil A > Crude Oil C).
4. The relative fouling rates parallel operational experience.
5. Characterization of a fouling deposit suggested that coking was the dominant fouling mechanism at these experimental conditions. The characterization results also suggest that sedimentation and corrosion were significant.
6. The carbonaceous portion of the fouling deposit was graphitic in nature but not true graphite.

ACKNOWLEDGMENT

NOMENCLATURE

A	Pre-exponential factor, m^2 K/kJ
CII	Colloidal instability index, dimensionless
$(dR_f/dt)_{ini}$	Initial fouling rate, m^2 K/kJ
E	Apparent activation energy, kJ/mol
Pr	Prandtl number, dimensionless
q	Heat flux, W/m^2
R	Universal gas constant, 8.314 J/mol K
Re	Reynolds number, dimensionless
R_f	Fouling resistance, m^2 K/W
R_s	Sheath resistance to heat transfer, m^2 K/W
t	Time, s
T_b	Average bulk fluid temperature, K
T_{imb}	Imbedded thermocouple temperature, K
T_{iso}	Isokinetic temperature, K
T_s	Sheath surface temperature, K
$T_{s,ini}$	Initial surface temperature, K
V	Velocity, m/s

Greek

α	Constant in Equation (1), dimensionless

REFERENCES
Bennett, C. A., Appleyard, S., Gough, M., Hohmann, R. P., Joshi, H. M., King, D. C., Lam, T. Y., Rudy, T. M., and Stomierowski, S. E., 2006, Industry-recommended procedures for experimental crude oil preheat fouling research, *Heat Trans. Eng.*, Vol. 27(9), pp. 28 – 35.

Bhatti, M. S. and Shah, R. K., 1987, Turbulent and transition flow convective heat transfer in ducts, in *Handbook of Single-Phase Convective Heat Transfer*, eds. Kakac, S., Shah, R. K., and Aung, W., Wiley, New York, pp. 4-116 – 4-117.

Fan, Z. and Watkinson, A. P., 2006, Formation and characteristics of carbonaceous deposits from heavy hydrocarbon coking vapors, *Ind. Eng. Chem. Res.*, Vol. 45, pp. 6428 – 6435.

Kane, R. D., 2006, Corrosion in petroleum refining and petrochemical operations, in *ASM Handbook Volume 13C, Corrosion: Environments and Industries*, eds. Cramer, S. D., and Covino, B. S., ASM International, Materials Park, Ohio, USA, pp. 981.

Linert, W., Kudrjawtsev, A. B., and Schmid, R., 1983, Concerning the problem of the isokinetic relationship. I. A statistical mechanical model, *Aust. J. Chem.*, Vol. 36, pp. 1903 – 1912.

Olmstead, W. N. and Freund, H., 1998, Thermal conversion kinetics of petroleum residua, in *Proceedings of the American Institute of Chemical Engineers Spring National Meeting*, New Orleans, Louisiana, USA.

Panchal, C. B., 1995, Fouling mitigation in the petroleum industry: where do we go from here?, in *Proceedings of Engineering Foundation Conference on Fouling Mitigation in Industrial Heat Exchangers*, San Luis Obispo, California, USA.

Park, C., Tan, C. D., Hidalgo, R., Baker, R. T. K., and Rodriguez, N. M., 1998, Hydrogen storage in graphite nanofibers, *Proceedings of the 1998 U.S. DOE Hydrogen Program Review (NREL/CP-570-25315)*.

Por, N., 1992, *Stability Properties of Petroleum Products*, The Israel Institute of Petroleum and Energy, The School of Petroleum and Energy Sciences.

Savage, P. E., Klein, M. T., and Kukes, S. G., 1985, Asphaltene reaction pathways. 1. Thermolysis, *Ind. Eng. Chem. Res.*, Vol. 24, pp. 1169 – 1174.

Schneider, R., and Mayr, H., 1986, Direct measurement of the "isokinetic rate constant" in additions of diarylcarbenium ions to 2-methyl-2-butene, *Angew. Chem. Int. Ed. Engl.*, Vol 25(11), pp. 1016 – 1017.

Somorjai, G. A., 1994, *Introduction to surface chemistry and catalysis*, Wiley, New York.

Watkinson, A. P., 2007, Deposition from crude oils in heat exchangers, *Heat Trans. Eng.*, Vol. 28(3), pp. 177 – 184.

Wiehe, I. A., 1992, A solvent-resid phase diagram for tracking resid conversion, *Ind. Eng. Chem. Res.*, Vol. 31, pp. 530 – 536.

Wiehe, I. A., 1993, A phase-separation kinetic model for coke formation, *Ind. Eng. Chem. Res.*, Vol. 32, pp. 2447 – 2454.

Wiehe, I. A., and Kennedy, R. J., 2000a, The oil compatibility model and crude oil incompatibility, *Energy & Fuels*, Vol. 14, pp. 56 – 59.

Wiehe, I. A., and Kennedy, R. J., 2000b, Application of the oil compatibility model to refinery streams, *Energy & Fuels*, Vol. 14, pp. 60 – 63.

Wiehe, I. A., 2001, The chemistry of petroleum fouling, American Institute of Chemical Engineers Spring National Meeting, Houston, Texas, USA.

Wilson, E. E., 1915, A basis for rational design of heat transfer apparatus, *Trans. ASME*, Vol. 37, pp. 47 – 82.

Yeap, B. L., Wilson, D. I., Polley, G. T., and Pugh, S. J., 2004, Mitigation of crude oil refinery heat exchanger fouling through retrofits based on thermo-hydraulic models, *Chem. Eng. Res. Des.*, Vol. 82(A1), pp. 53 – 71.

Yelon, A., Movaghar, B., and Crandall, R. S., 2006, Multi-excitation entropy: its role in thermodynamics and kinetics, *Rep. Prog. Phys.*, Vol. 69, pp. 1145 – 1194.